

Interstellar Neutral Gas Species And Their Pickup Ions Inside The Heliospheric Termination Shock.  
Ionization Rates For H, O, Ne, And He.JUSTYNA M. SOKÓŁ,<sup>1</sup> MACIEJ BZOWSKI,<sup>1</sup> AND MUNETOSHI TOKUMARU<sup>2</sup><sup>1</sup>*Space Research Centre, Polish Academy of Sciences, (CBK PAN), Warsaw, Poland*<sup>2</sup>*Institute for Space-Earth Environmental Research, Nagoya University, Nagoya, Japan*

(Received September 27, 2018; Revised –; Accepted –)

Submitted to ApJ

## ABSTRACT

Solar ionizing factors, corpuscular and electromagnetic radiation, are key factors to understand the modulation of interstellar neutral gas and its derivative populations inside the heliosphere. In the present paper we overview the current state of the knowledge about the solar ionizing factors for the heliospheric particles inside the termination shock. We discuss charge exchange with solar wind particles, photoionization, and electron impact ionization as the most relevant ionization processes. We compare the ionization rates for hydrogen, oxygen, neon, and helium for the last three cycles of solar activity (from 1985 to 2018) both in the ecliptic plane and in the polar regions. We discuss relations between ionization processes for a given species as a function of time, solar distance, and latitude. We study similarities and differences of the total ionization rates among the species within a consistent and homogeneous system of calculation of the ionization rates for heliospheric particles inside the heliosphere. Among the species discussed, the highest total ionization rates at 1 au in the ecliptic plane are for hydrogen and oxygen, and the lowest are for helium. In the polar regions, the strongest ionization losses are for oxygen, regardless of the phase of the solar activity. Photoionization is the dominant ionization reaction for helium and neon, and a reaction of high significance for oxygen. Charge exchange with solar wind particles is the dominant ionization reaction for hydrogen and the second important ionization reaction for oxygen. Electron impact ionization is an important ionization reaction for Ne and He, with the contribution to the total ionization rates stronger within 1 au and smaller outside 1 au. The total ionization rates for He and Ne vary significantly in time with the solar activity, whereas the total ionization rates for H and O follow the cyclic solar wind variations out of the ecliptic plane and aperiodic variations in the ecliptic plane.

**Keywords:** astroparticle physics — Sun: activity — Sun: heliosphere — (Sun:) solar wind — ISM: kinematics and dynamics

## 1. INTRODUCTION

The heliospheric particles, like pickup ions (PUIs) and energetic neutral atoms (ENAs), and heliospheric phenomena, like the resonant backscatter glow in the solar hydrogen (121.6 nm) and helium (58.4 nm) lines, result from interaction of the interstellar medium with the solar output inside the heliosphere. The interstellar neutral (ISN) particles enter the heliosphere unaffected by

the magnetic field, and during their travel inside the heliosphere they are exposed to the solar ionizing factors, like collisions with solar wind particles (protons, alphas, and electrons) and solar extreme ultraviolet (EUV) radiation. In consequence of ionization of ISN particles, new populations of particles are created. In general, ionization of ISN gas creates PUIs, charge exchange reaction of PUIs and neutral solar wind create various populations of ENAs. ISN gas, PUIs, and ENAs can reach close distances to the Sun and be sampled by heliospheric space probes like, e.g., IBEX (McComas et al. 2009), Ulysses (Wenzel et al. 1989; Witte et al. 1992), New Horizons

(McComas et al. 2008a), Cassini (Young et al. 2004), to list only a few. All of the heliospheric particles interact with the solar output and undergo losses due to ionization processes. Thus, the knowledge on the solar ionization factors and their modulation in time and with solar distance and latitude is fundamental in the study of ISN gas distribution, PUI production rate, and the physics of ENAs in the heliosphere.

Studies of ISN gas, enabled by measurements from inside the heliosphere, allow to infer the velocity vector of the heliosphere's motion with respect to the Local Interstellar Medium (LISM; e.g., Bzowski et al. (2015)) and bring information about the physical state of the LISM including temperature (e.g., Bzowski et al. 2014; McComas et al. 2015) and elemental composition (e.g., Park et al. 2014). Moreover, the ISN gas flow vector can be studied indirectly by the measurement of PUIs (e.g., Möbius et al. 2015). The physical processes in the inner and outer heliosheath may be studied via measurements of ENAs (see, e.g., a comprehensive review by Zank (2015)). In all the cases a careful accounting for the solar ionization factors is needed to deconvolve the solar modification of the particle fluxes on their way from the source region to the instruments close to the Sun from the modulation in the source region to correctly interpret the measurements (Bzowski 2008; McComas et al. 2012).

This paper belongs to a series “*Interstellar Neutral Gas Species And Their Pickup Ions Inside The Heliospheric Termination Shock*,” in which topics related with the study and modeling of ISN gas and PUIs inside the heliosphere are discussed. Here we summarize our current state of knowledge about the solar ionizing factors for heliospheric particles inside the heliosphere. We discuss the most relevant ionization processes for heliospheric particles, including charge exchange with solar wind protons and alpha particles, impact ionization by solar wind electrons, and ionization by the solar EUV radiation. We apply a homogeneous system of calculation of ionization losses for heliospheric particles relevant for the study of ISN gas, PUIs, and ENAs inside the heliosphere developed in our previous studies. The system is built on currently best available solar observations. We compare the ionization rates for the four most abundant ISN species inside the heliosphere. We study relations of the ionization rates among different species, we discuss similarities and differences and the resulting consequences for heliospheric studies. The ionization rates described here are next used to calculate the density of the ISN gas and the production rate for PUIs through-

out the heliosphere, discussed in Sokół et al. (0000a)<sup>1</sup>, Sokół et al. (0000b)<sup>2</sup>, and Sokół et al. (0000c)<sup>3</sup>.

We consider ionization rates for interstellar particles of hydrogen, oxygen, neon, and helium in the inner heliosphere. The ionization losses discussed here are a function of time, solar distance, and latitude. We study the solar ionizing factors backward in time as long as observational data are available. We discuss the ionization rates averaged in time over Carrington rotation periods<sup>4</sup>.

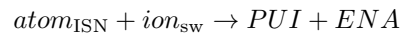
The paper is organized as follows: a brief description of ionization reactions relevant for the study of heliospheric particles together with references to the currently used models is presented in Section 2. Relations between total ionization rates for various species are discussed in Section 3. We summarize the study in Section 4.

## 2. IONIZATION PROCESSES

The interaction of heliospheric particles with the solar medium is via charge exchange with solar wind protons and alpha particles ( $\beta_{cx}$ , Section 2.1), photoionization by the solar EUV radiation ( $\beta_{ph}$ , Section 2.2), and the impact ionization by solar wind electrons ( $\beta_{el}$ , Section 2.3). The ionization processes for the ISN gas were discussed in detail by Ruciński et al. (1996, 1998); Fahr et al. (2007), a review can be also found in Bzowski et al. (2013b), and we reference reader therein. An overview of the ionization processes relevant for heliospheric particles, but in the heliosheath, can be found in Scherer et al. (2014).

### 2.1. Charge exchange

Charge exchange is a reaction in which a charge (electron) is captured by ion (in our case proton or alpha particle) from atom:



The intensity of charge exchange ionization for ISN atoms is a function of concentration of the impacting

<sup>1</sup> Sokół et al., *Interstellar Neutral Gas Species and Their Pickup Ions Inside The Heliospheric Termination Shock. Basics of modeling*, in preparation

<sup>2</sup> Sokół et al., *Interstellar Neutral Gas Species And Their Pickup Ions Inside The Heliospheric Termination Shock. The Large-scale Structures*, in preparation

<sup>3</sup> Sokół et al., *Interstellar Neutral Gas Species And Their Pickup Ions Inside The Heliospheric Termination Shock. The Solar Cycle Variations and Modulation At Termination Shock*, in preparation

<sup>4</sup> Carrington rotation is the mean synodic rotation period of 27.2753 days.

component, relative velocity of the reacting particles, and the cross-section for the reaction, as given by Equation 1:

$$\beta_{\text{cx}}(t, r, \phi) = n_{\text{sw}}(t, r, \phi) v_{\text{rel}}(t, r, \phi) \sigma_{\text{cx}}(v_{\text{rel}}(t, r, \phi)), \quad (1)$$

with

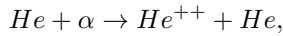
$$v_{\text{rel}}(t, r, \phi) = |\vec{v}_{\text{atom}}(t, r, \phi) - \vec{v}_{\text{sw}}(t, r, \phi)|,$$

where  $\vec{v}_{\text{atom}}$  is the velocity of an ISN atom,  $\vec{v}_{\text{sw}}$  is the solar wind velocity, assumed to flow radially,  $n_{\text{sw}}$  is the concentration of solar wind particles (protons or alpha particles, depending on the reaction), and  $\sigma_{\text{sw}}$  is the cross-section for charge exchange. We assumed that the solar wind varies in time ( $t$ ), solar distance ( $r$ ), and latitude ( $\phi$ ). For the distance dependence we adopt decrease with the square of solar distance for the solar wind density and independence with distance for the solar wind velocity:

$$n_{\text{sw}}(r) = n_{\text{sw}}(r_0) \left(\frac{r_0}{r}\right)^2, \quad v_{\text{sw}}(r) = v_{\text{sw}}(r_0), \quad (2)$$

where  $r_0 = 1$  au.

We use the charge exchange cross-sections after Lindsay & Stebbings (2005) for H and O, Nakai et al. (1987) for Ne, and Barnett et al. (1990) for He. In the case of helium atoms, the charge exchange ionization reaction, in addition to charge exchange with protons, may be due to interaction with the alpha particles:

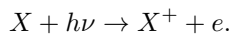


which we account for in our calculations. Thus, the charge exchange rate for He presented further is a sum of charge exchange reactions with protons and alpha particles.

To calculate the charge exchange rates, we use the model of the solar wind evolution in time and latitude developed by Sokół et al. (2013). The model is based on in-ecliptic multi-spacecraft solar wind data from the OMNI collection and indirect solar wind observations via the interplanetary scintillations (IPS). More about the solar wind data used can be found in Section 2.4. For the calculation of charge exchange with alpha particles we adopted a constant fraction of alpha particles in the solar wind equal to 4% of the proton number density.

## 2.2. Photoionization

Photoionization is an ionization via knock out of electron from atom by photons:



A particle can be ionized by photons with the energies higher than the threshold energy for a given species: 13.6 eV for H, 24.6 eV for He, 13.6 eV for O, and 21.6 eV for Ne. These energies require photons of wavelengths equal to or smaller than 91.2 nm, 50.4 nm, 91.1 nm, and 57.5 nm, respectively. This makes the EUV spectral range of the solar electromagnetic radiation the main source of photoionization for heliospheric particles.

Photoionization rate is calculated by integration of the measured solar spectral EUV flux ( $F_{\text{EUV}}$  in units of  $\text{W m}^{-2} \text{nm}^{-2}$ ) in a given wavelength ( $\lambda$ ) multiplied by the cross-section for photoionization ( $\sigma_{\text{ph}}$ ), as given in Equation 3:

$$\beta_{\text{ph}}(t) = (hc)^{-1} \int_0^{\lambda_0} \lambda F_{\text{EUV}}(\lambda, t) \sigma_{\text{ph}}(\lambda) d\lambda, \quad (3)$$

where  $\lambda_0$  is wavelength for the ionization threshold for a given atom. The cross-sections for photoionization are adopted from Verner et al. (1996).

The EUV flux is modulated by the distribution of active sources on the solar surface, however, as shown by McMullin et al. (2004), the latitudinal variation of the photoionization rates is expected to be moderate (but this topic requires further studies). In this study, we approximated the latitudinal variations by an educated guess formula (Bzowski 2008; Bzowski et al. 2013b):

$$\beta_{\text{ph}}(\phi) = \beta_{\text{ph}}(0^\circ) (0.85 \sin^2(\phi) + \cos^2(\phi)). \quad (4)$$

The heliospheric environment is optically thin for the ionizing photons, thus for the distance dependence of photoionization, we can adopt the following relation:

$$\beta_{\text{ph}}(r) = \beta_0 \left(\frac{r_0}{r}\right)^2. \quad (5)$$

To calculate photoionization rates, we used the methodology described by Bzowski et al. (2013b,a) to create a composite series of photoionization rates based on the available data of the solar EUV flux and solar EUV proxies (see also Bochsler et al. 2014). The solar EUV flux comes from the TIMED/SEE data (Level 3, Version 11; Woods et al. 2005). For solar EUV proxies we used the flux measured by SOHO/CELIAS/SEM (Judge et al. 1998; Wieman et al. 2014), F10.7 radio flux (Tapping 1987, 2013), the Magnesium index ( $\text{Mg}_{c/w}$ , Snow et al. 2014), and the composite Lyman- $\alpha$  flux released by LASP (Woods et al. 1995). Details of the construction of the photoionization rates can be found in Sokół & Bzowski (2014) for He, Bzowski et al. (2013a); Sokół et al. (2016) for Ne and O, and Bzowski et al. (2013b) for H.

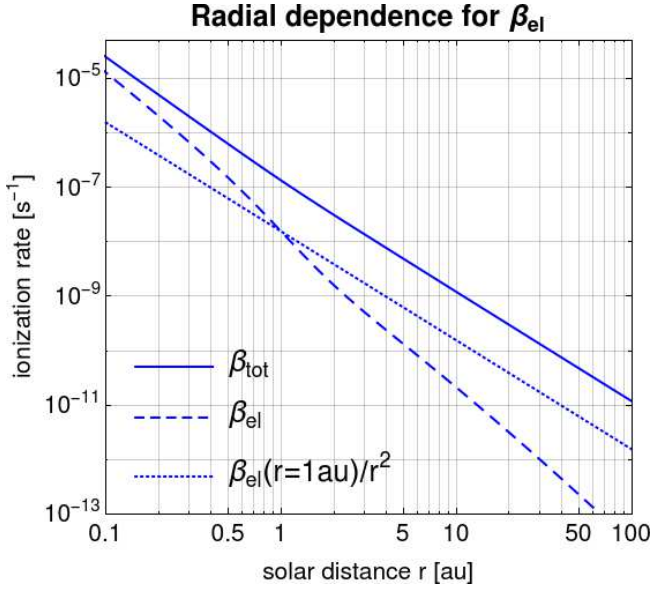
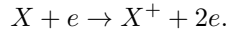


**Figure 1.** Departure of the electron impact ionization rate from the  $r^{-2}$  decrease with the solar distance shown as example for He for the slow solar wind. Solid line presents the radial dependence of total ionization rates. Dashed line presents the radial dependence following the [Bzowski \(2008\)](#) methodology. Dotted line illustrates the  $r^{-2}$  decrease of the 1 au electron impact ionization rate. The rates shown for a moderate solar activity, as in 1999.

### 2.3. Electron impact ionization

Electron impact ionization is a reaction in which an electron knocks out another electron from an atom:



The electron impact ionization includes two populations of solar wind electrons, approximated by a two-Maxwellian distribution (including core and halo populations;  $f_{el}(E, t, r, \phi)$ ) and, in general, is calculated as given in Equation 6:

$$\beta_{el}(t, r, \phi) = \int_{E_i}^{\infty} f_{el}(E, t, r, \phi) \sigma(E) E dE, \quad (6)$$

where  $\sigma_{el}$  is the cross-section for electron impact ionization, adopted in our study from [Lotz \(1967\)](#).

We calculate the electron impact ionization following the methodology proposed by [Ruciński & Fahr \(1989, 1991\)](#) and developed by [Bzowski \(2008\)](#); [Bzowski et al. \(2013a\)](#) based on Ulysses and Helios measurements. Details of the electron impact ionization for ISN H are given by [Bzowski \(2008\)](#) and for ISN He, Ne, and O by [Bzowski et al. \(2013a\)](#). In the present study we limit the electron impact ionization to the slow solar wind regime for all latitudes, which results in overestimation

of the electron impact ionization rates for polar regions (see Figures 9 and 10 in [Bzowski \(2008\)](#)). However, due to small fractional input of electron impact ionization to the total ionization rates for the discussed species (see, e.g., Table 1) this simplification does not seriously impact the results discussed, because the fractional input of electron impact ionization rates to the total ionization rates is comparable to the accuracy of the total ionization rates model (see discussion in [Bzowski et al. \(2013a\)](#)).

Unlike the charge exchange ionization and photoionization, the electron impact ionization decreases with the solar distance faster than  $r^{-2}$ :

$$\beta_{el}(r) \neq \beta_0 \left(\frac{r_0}{r}\right)^2.$$

This is a consequence of faster cooling of solar wind electron fluid with the solar distance. Figure 1 compares the distance dependence of electron impact ionization decrease with the  $r^{-2}$  decrease in the case of helium.

### 2.4. Solar wind latitudinal structure

Charge exchange and electron impact ionization rates depend on the solar wind speed and density and, in consequence, they vary with heliographic latitude during the solar cycle as the solar wind does (more in Section 3.2). Additionally, they follow the long-term changes in the solar wind observed in the recent decades (Section 3.1; [McComas et al. \(2008b\)](#); [Sokół et al. \(2013\)](#); [McComas et al. \(2018b\)](#); [Tokumaru et al. \(2018\)](#)).

We adopt the solar wind structure in and out of the ecliptic plane and its evolution during solar cycle after [Sokół et al. \(2013\)](#). The methodology described in [Sokół et al. \(2013\)](#) was applied to data covering the time range from 1985 to 2018, as presented in Figure 2. The time resolution is one Carrington rotation. In the ecliptic plane, the model is based on multi-spacecraft observations of the solar wind available through the OMNI database ([King & Papitashvili 2005](#)). For the solar wind structure out of the ecliptic plane, we adopted the solar wind speed retrieved from the IPS observations conducted by the Institute for Space-Earth Environmental Research (ISEE, Nagoya University, Japan; [Tokumaru et al. \(2010, 2012, 2015\)](#)). The solar wind density is calculated with the use of the speed-density relation as derived from fast orbital scans of Ulysses/SWOOPS and from the latitudinally invariant solar wind advection energy flux ([Le Chat et al. 2012](#)), as described in [Sokół et al. \(2015\)](#) and Appendix B in [McComas et al. \(2014\)](#).

The solar wind data we used cover the last three solar cycles (SC), it is SC 22 (Sep 1986 – Aug 1996), SC 23



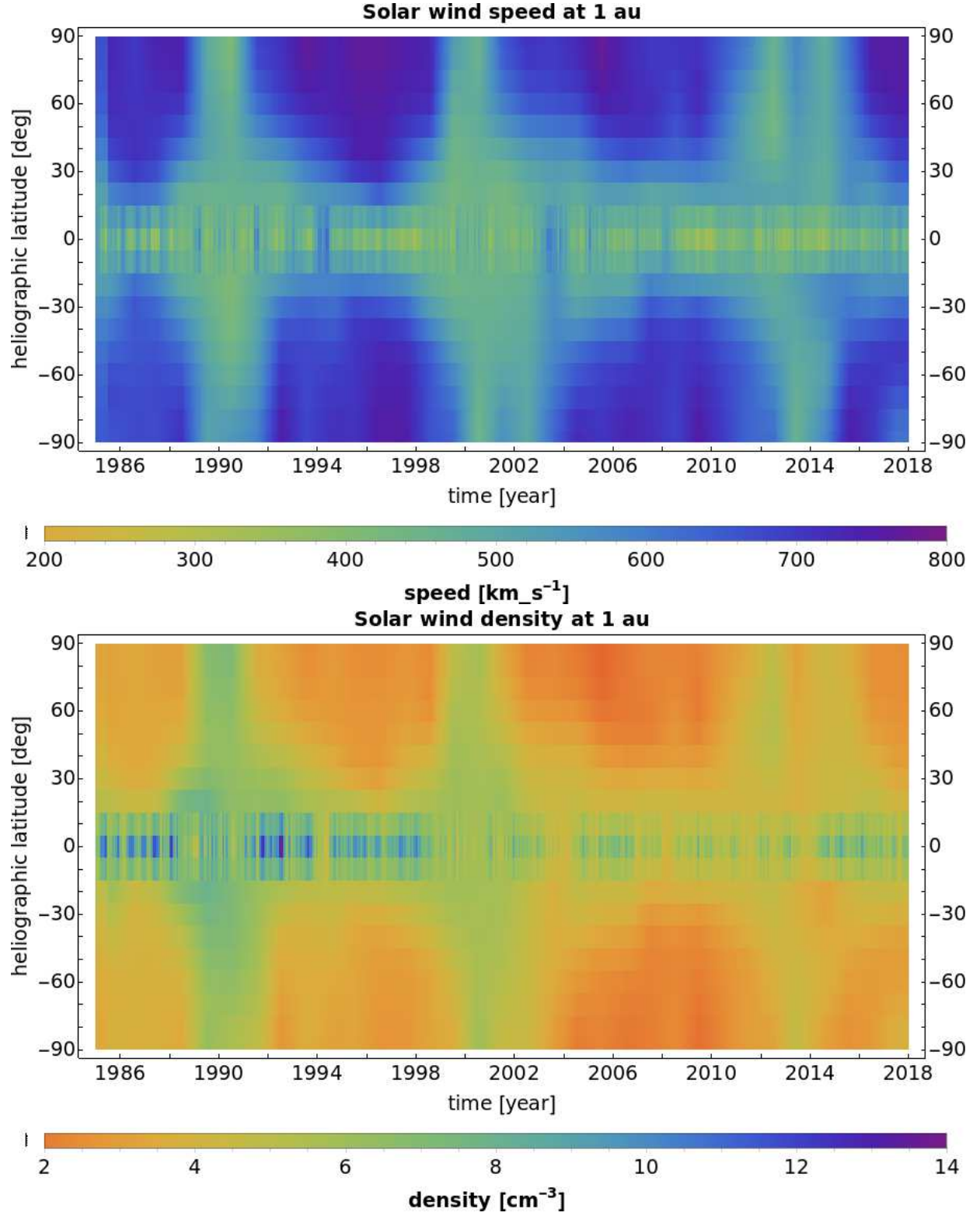


**Figure 2.** Top: solar wind speed at 1 au as a function of time and heliographic latitude obtained following the methodology described by [Sokół et al. \(2013\)](#). Bottom: solar wind density at 1 au as a function of time and heliographic latitude calculated based on the methodology described by [Sokół et al. \(2013, 2015\)](#) and [McComas et al. \(Appendix B; 2014\)](#)

(Aug 1996 – Dec 2008), SC 24 (Dec 2008 – Apr 2018)), as presented in Figure 2. The solar wind speed and density is almost uniform during a short time period during the maximum of solar activity (around 1990, 2001, 2013–2014), with the slow flow of speed about  $450 \text{ km s}^{-1}$  and density about  $6 \text{ cm}^{-3}$ . During other phases of solar activity (decreasing, minimum, and increasing), the slow and dense wind flows are restricted to lower latitudes, with limitation to a band of  $\pm 30^\circ$  around solar equator during solar minimum. In the same time, at higher latitudes the flow is fast, with a speed about  $750 \text{ km s}^{-1}$  and with the density about twice lower than the equatorial flow.

### 2.5. Radiation pressure

The gravitational focusing and ionization are the two main modifying factors for the heliospheric particles inside the heliosphere. However, in the case of hydrogen atoms, an important role also plays the radiation pressure by solar Lyman- $\alpha$  photons, which modifies the net force acting on the hydrogen atoms in the heliosphere (Tarnopolski & Bzowski 2009). The radiation pressure is the most effective for hydrogen atoms among the species discussed, for other species it is negligible (Ruciński 1985).

We adopt in our calculations the radiation pressure model of the solar Lyman- $\alpha$  flux on ISN H developed recently by Kowalska-Leszczynska et al. (2018a,b).

## 3. TOTAL IONIZATION RATES

The effective ionization rate for the heliospheric particles is a sum of the rates of all three ionization processes discussed

$$\beta_{\text{tot}} = \beta_{\text{cx}} + \beta_{\text{ph}} + \beta_{\text{el}}. \quad (7)$$

All three ionization reactions discussed in Section 2 vary in time, solar distance, and latitude. However, these variations are of different significance for a given ionization process. The charge exchange rate varies significantly as a function of latitude due to the fast/slow solar wind flow variations during the solar cycle (Figure 2). Also reflected in the charge exchange rates are the long-term variations of the solar wind dynamic pressure, weakly correlated with the phase of the solar cycle (Figure 3). Photoionization is the ionization reaction that shows the strongest variation with the solar activity, but most likely not with latitude, and thus the variations in time are the main driver of its modulation (Figure 3). The electron impact ionization varies in latitude as the solar wind does, however the key parameter for its modulation inside the heliosphere is its solar distance variation (Figure 1, 3, 4). This latter factor makes

the electron impact ionization reaction the most significant at close distances to the Sun (within 1 au) and almost negligible elsewhere inside the solar wind termination shock, as illustrated in Figure 4.

In further discussion we focus on relations between the ionization rates for H, O, Ne, and He at 1 au and out of the ecliptic plane for the time period from 1985 to 2018 (SC 22, 23, 24) with resolution in time equal to the Carrington rotation.

### 3.1. In-ecliptic variation

Various ionization processes affect interstellar species in different ways, resulting in different modulations of the heliospheric particles inside the heliosphere and, in consequence, in different density distributions and PUI production rates (Sokół et al. 0000b,c). Most of the available measurements of the heliospheric particles (ISN gas, PUIs, ENAs) are collected by instruments operating in the ecliptic plane and at 1 au. Thus, the variation of the ionization rates close to the ecliptic at 1 au are of high significance for the heliospheric studies and very often serve as a reference for the ionization rates inside the heliosphere. However, because the trajectories of particles measured in the ecliptic plane traverse the heliosphere at different latitudes, the latitudinal variation of ionization rates cannot be neglected, especially in studies of the ISN cone and the downwind hemisphere (see Section 3.2 and discussion in Sokół et al. (2016, 0000b)).

Figure 3 compares the in-ecliptic time series of the ionization rates for H, O, Ne, and He at 1 au from 1985 to 2018. All three ionization reactions are presented together with the total ionization rate for a given species. The bottom panels of Figure 3 present the fraction of a given ionization reaction to the total ionization rate. The average of these fractional contributions is summarized in Table 1. The values presented are averages over all Carrington rotations in the period from 1985 to 2018. In addition, we present standard deviations as well as the minimal and the maximal fractional input of an individual ionization reaction to the total ionization rate for the discussed period in time.

Hydrogen is the most prone to charge exchange with the solar wind protons, which constitutes on average 76% of the total ionization rate for this species (Figure 3 and Table 1). The remaining ionization reactions for H, photoionization and electron impact ionization, bring up to 16% and 8% to the total ionization losses, respectively. Moreover, ISN H is significantly affected by the Lyman- $\alpha$  radiation pressure (see Kowalska-Leszczynska et al. 2018a,b), which has impor-

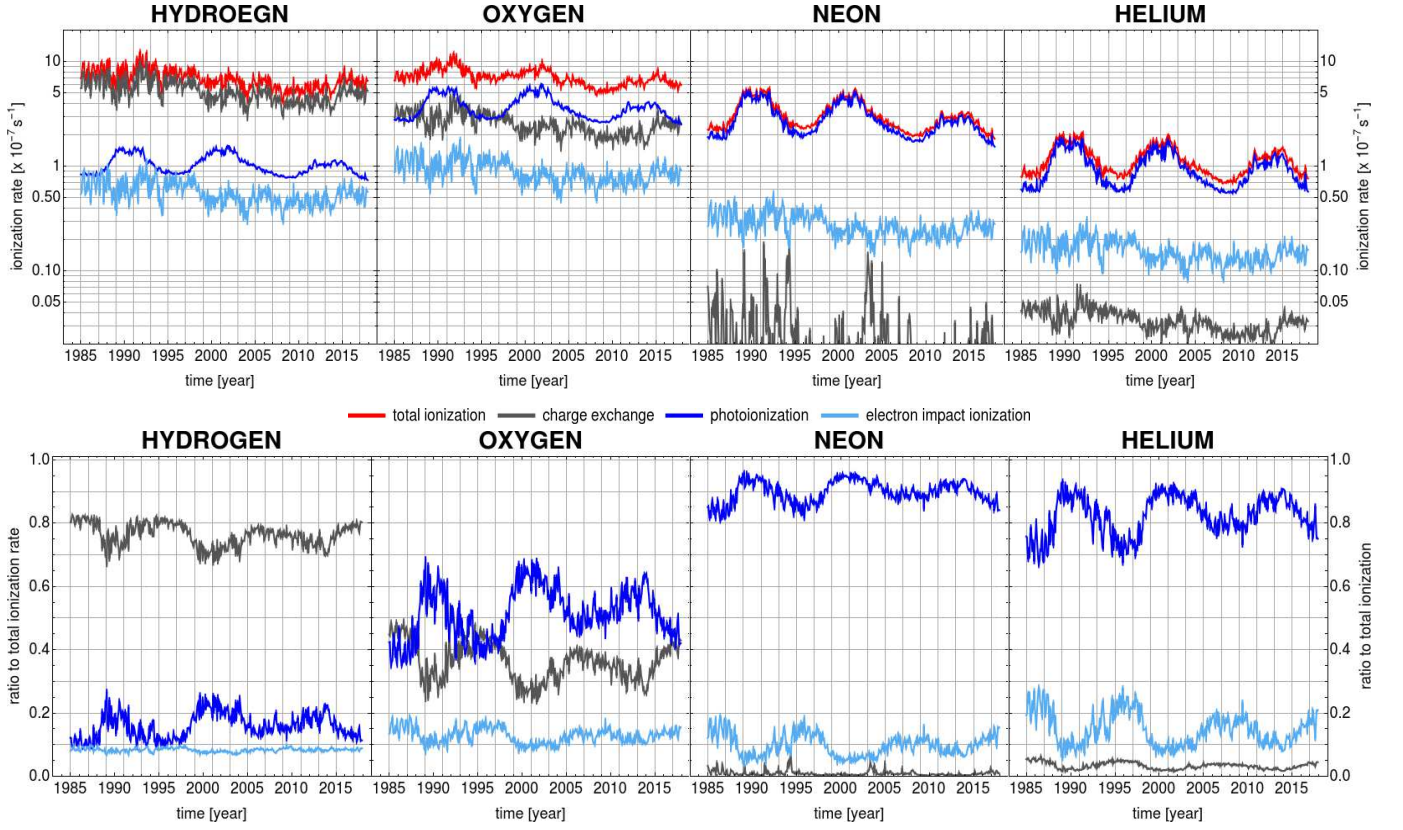


**Figure 3.** Top: Time series of ionization rates due to various ionization processes for H, O, Ne, and He in the ecliptic plane at 1 au with Carrington rotation resolution in time. Bottom: Time series of the ratios of the individual ionization reaction rates to the total ionization rates for a given species. The color code is given between the two rows of panels.

**Table 1.** Ratios of charge exchange ionization, photoionization, and electron impact ionization rates to the total ionization rates for H, O, Ne, and He at 1 au in the ecliptic plane, averaged over a period from 1985 to 2018.

$\beta_*/\beta_{\text{tot}}$ : min $\leq$ <b>mean</b> $\pm \sigma$ $\leq$ max			
...	Charge exchange	Photoionization	Electron impact
hydrogen	$0.67 \leq \mathbf{0.76} \pm \mathbf{0.04} \leq 0.83$	$0.09 \leq \mathbf{0.16} \pm \mathbf{0.04} \leq 0.27$	$0.07 \leq \mathbf{0.08} \pm \mathbf{0.01} \leq 0.10$
oxygen	$0.23 \leq \mathbf{0.36} \pm \mathbf{0.06} \leq 0.49$	$0.35 \leq \mathbf{0.51} \pm \mathbf{0.08} \leq 0.68$	$0.07 \leq \mathbf{0.13} \pm \mathbf{0.02} \leq 0.19$
neon	$0.001 \leq \mathbf{0.008} \pm \mathbf{0.008} \leq 0.072$	$0.805 \leq \mathbf{0.896} \pm \mathbf{0.035} \leq 0.958$	$0.035 \leq \mathbf{0.096} \pm \mathbf{0.034} \leq 0.190$
helium	$0.01 \leq \mathbf{0.03} \pm \mathbf{0.01} \leq 0.06$	$0.67 \leq \mathbf{0.82} \pm \mathbf{0.06} \leq 0.93$	$0.05 \leq \mathbf{0.15} \pm \mathbf{0.05} \leq 0.28$

tant consequences for the ISN H and  $\text{H}^+$  PUI distribution (more in Sokół et al. (0000b,c)).

The other species for which the charge exchange with the solar wind particles is significant is oxygen. Typically, however, charge exchange constitutes only about 36% of the total ionization rate for oxygen, whereas photoionization brings on average about 51%. But, as presented in Figure 3, the relative input from the two reactions is strongly variable and can be comparable like, e.g., in 1996 or 2017, which corresponds to the minimum of the solar activity. An exception is the minimum between SC 23 and SC 24, when the solar wind flux was low and the photoionization was responsible for  $\sim 50\%$

of the ionization for ISN O, with  $\sim 40\%$  due to charge exchange ionization and  $\sim 10\%$  due to electron impact ionization. The photoionization is the dominant ionization reaction for oxygen during the solar maximum regardless of the solar cycle epoch and is about two times higher than the charge exchange rate. The interplay between these two most effective ionization reactions for ISN O is modulated in time both by the periodic variations of the solar activity and by the long-term changes in the solar wind dynamic pressure.

For ISN He and Ne, the dominant ionization reaction is ionization by the solar EUV radiation (see Figure 3 and Table 1). Of second importance is electron impact

**Table 2.** Ratios of the total ionization rates for O, Ne, and He with respect to the total ionization rates for H at 1 au in the ecliptic plane and in the polar region, averaged over a period from 1985 to 2018. The polar ratio is an average for the south and north poles.

$\beta_{\text{tot}}(*) / \beta_{\text{tot}}(H)$ : min $\leq$ <b>mean</b> $\pm \sigma \leq$ max			
...	oxygen	neon	helium
in-ecliptic	$0.82 \leq \mathbf{1.06} \pm \mathbf{0.14} \leq 1.45$	$0.24 \leq \mathbf{0.47} \pm \mathbf{0.15} \leq 0.94$	$0.09 \leq \mathbf{0.17} \pm \mathbf{0.05} \leq 0.34$
polar	$1.09 \leq \mathbf{1.29} \pm \mathbf{0.11} \leq 1.57$	$0.43 \leq \mathbf{0.65} \pm \mathbf{0.11} \leq 0.96$	$0.14 \leq \mathbf{0.22} \pm \mathbf{0.04} \leq 0.33$

ionization, which is a little higher for Ne than for He, but brings more to the total ionization rates for He than for Ne. The electron impact ionization for He can bring to the total ionization rate at 1 au more than  $\sim 25\%$  during solar minimum, and as low as  $\sim 5\%$  during solar maximum. This fractional input of electron impact ionization to the total ionization rate for He increases for distances to the Sun smaller than 1 au, as presented in Figure 4. The charge exchange with solar wind particles is almost negligible for these two species. Because the solar EUV flux varies in time with the solar activity, the ionization losses for He and Ne also vary during solar cycle and are two-fold higher during solar maximum than during solar minimum (Figure 3).

A comparison among the species shows that in the ecliptic plane the highest ionization rates are for hydrogen and oxygen, for which the total ionization rates are almost identical as presented in Figures 3 and 8, and Table 2. The lowest ionization rates are for helium being less than 20% of the total ionization rate for hydrogen. The total ionization rate for neon is about 0.5 of the hydrogen total ionization rate.

Additionally, two groups among the ionization rates can be identified. One group which follows the solar cycle variations in time, like those for He and Ne. The other group includes those for which these variations are not directly reflected in the in-ecliptic rates, but are present out of the ecliptic plane, like in the case of H and O. This is because the solar wind in the ecliptic plane does not show a clear quasi-periodic variability related to the cycle of solar activity (Figure 2) and consequently, the total ionization rate of the species for which the charge exchange ionization dominates, also does not show a clear quasi-periodic solar cycle variations in the ecliptic plane (Figure 5). Since, however, solar wind features a clear solar cycle-related modulation in the polar regions, also the charge exchange rate for H and O in the polar regions is modulated in phase with the solar cycle, as further discussed in Section 3.2.

Considering ionization rates for heliospheric particles inside the heliosphere, the importance of the solar distance variations of the electron impact ionization cannot be neglected. Despite small contribution of this reaction to the total ionization rates, as presented in Figure 3, its

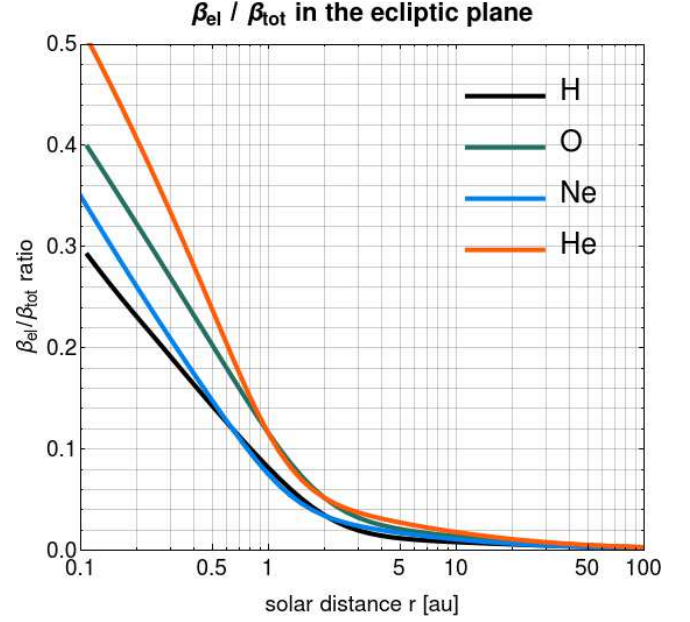


**Figure 4.** Ratio of the electron impact ionization to total ionization rates in the ecliptic plane as a function of solar distance for four species discussed for a moderate solar activity, as in 1999.

significance increases fast for distances to the Sun less than 1 au, as illustrated in Figure 4. The species most affected by electron impact ionization inside 1 au is helium, next oxygen and neon, and the smallest hydrogen. Thus, the future observations of the solar wind electron temperature at closer distance to the Sun expected from the Parker Solar Probe (Fox et al. 2016) and Solar Orbiter (<http://sci.esa.int/solar-orbiter/>) missions and the Global Solar Wind Structure (GLOWS) experiment onboard future IMAP mission (McComas et al. 2018a) can bring new insights to the currently poorly understood electron impact ionization and consequently the energetics of solar wind electrons inside 1 au.

### 3.2. Latitudinal variation

Due to the dependence on the solar wind conditions, the charge exchange and the electron impact rates ionization vary in latitude during the solar cycle as the solar wind flow does (Equations 1 and 6). The slow and dense solar wind spans all latitudes during the solar maximum (Figure 2) and in consequence the charge ex-



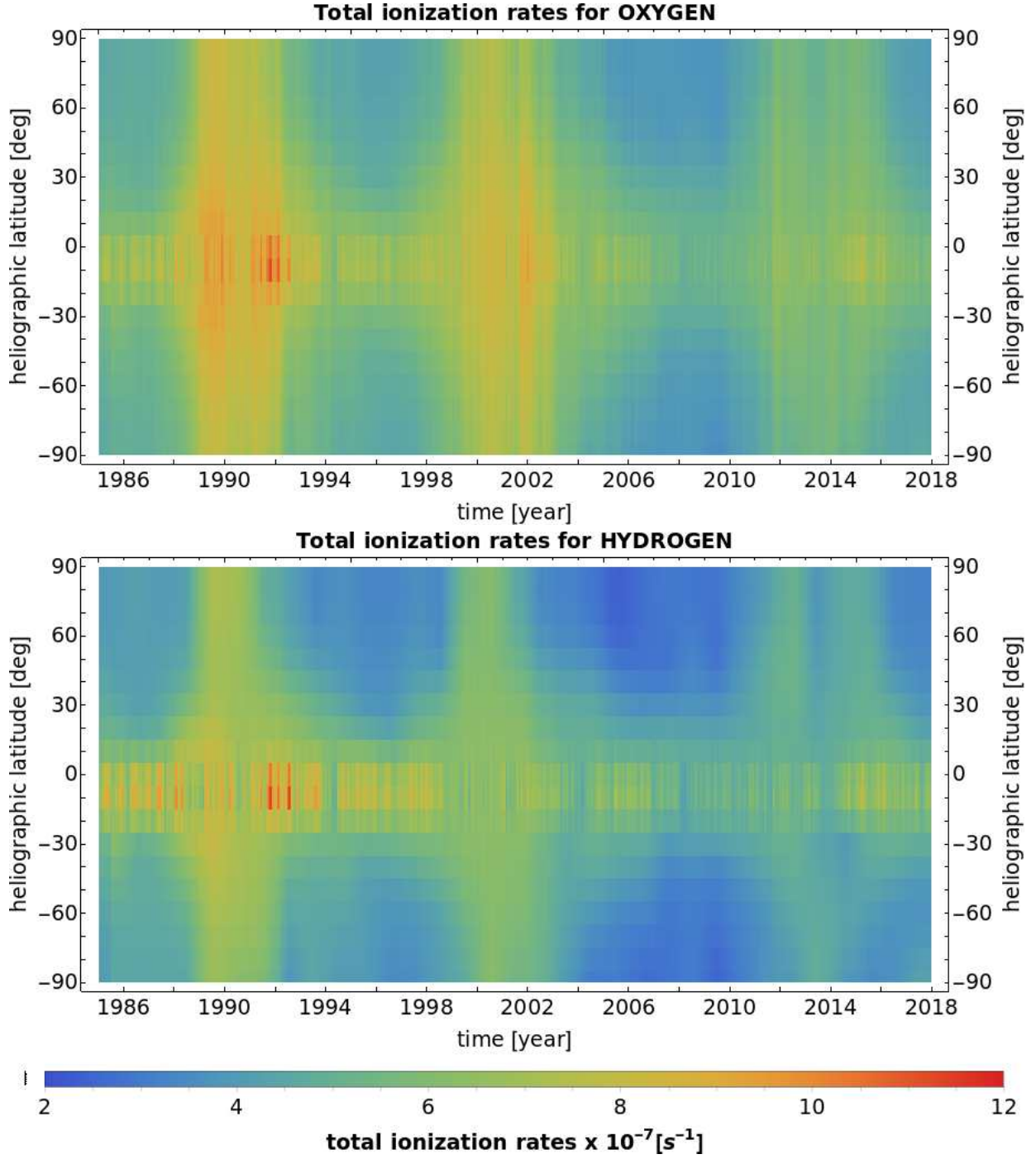


**Figure 5.** Total ionization rates at 1 au as a function of heliographic latitude and time for oxygen (top panel) and hydrogen (bottom panel). Color bar is common for both panels.

change is almost uniform as a function of latitude during solar maximum. During solar minimum and phases of decreasing and increasing solar activity, the solar wind has bi-modal structure in latitudes, with slow and dense flows limited to lower latitudes with a narrow band of about  $\pm 30^\circ$  around solar equator during solar minimum, and with fast and dilute flows at higher latitudes. This bi-modal structure is reflected in latitudinal variations

of the charge exchange and electron impact ionization rates, and, in consequence, in the total ionization rates for species prone to these two ionization process (Figure 2 and Figure 5).

Because charge exchange is the dominant ionization reaction for hydrogen and oxygen (Figure 3, Table 1), the effective total ionization rates for these species vary significantly with latitude during the solar cycle, as pre-

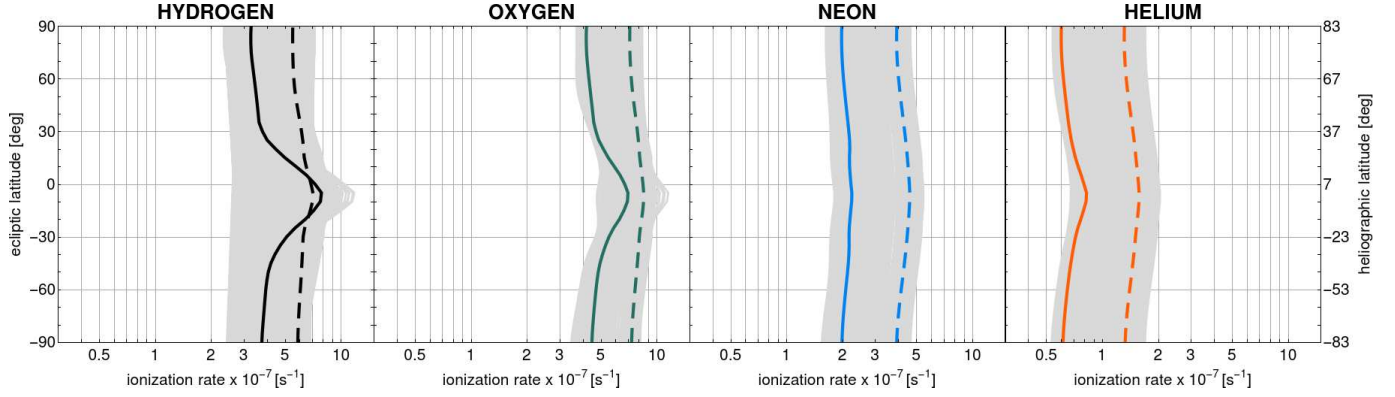


**Figure 6.** Total ionization rates at 1 au as a function of ecliptic (heliographic) latitude at 1 au during solar minimum ( $\sim 1996$ , solid line) and solar maximum ( $\sim 2001$ , dashed line). The gray shadows mark the region occupied by the latitudinal profiles for all Carrington rotations in the period from 1985 to 2018.

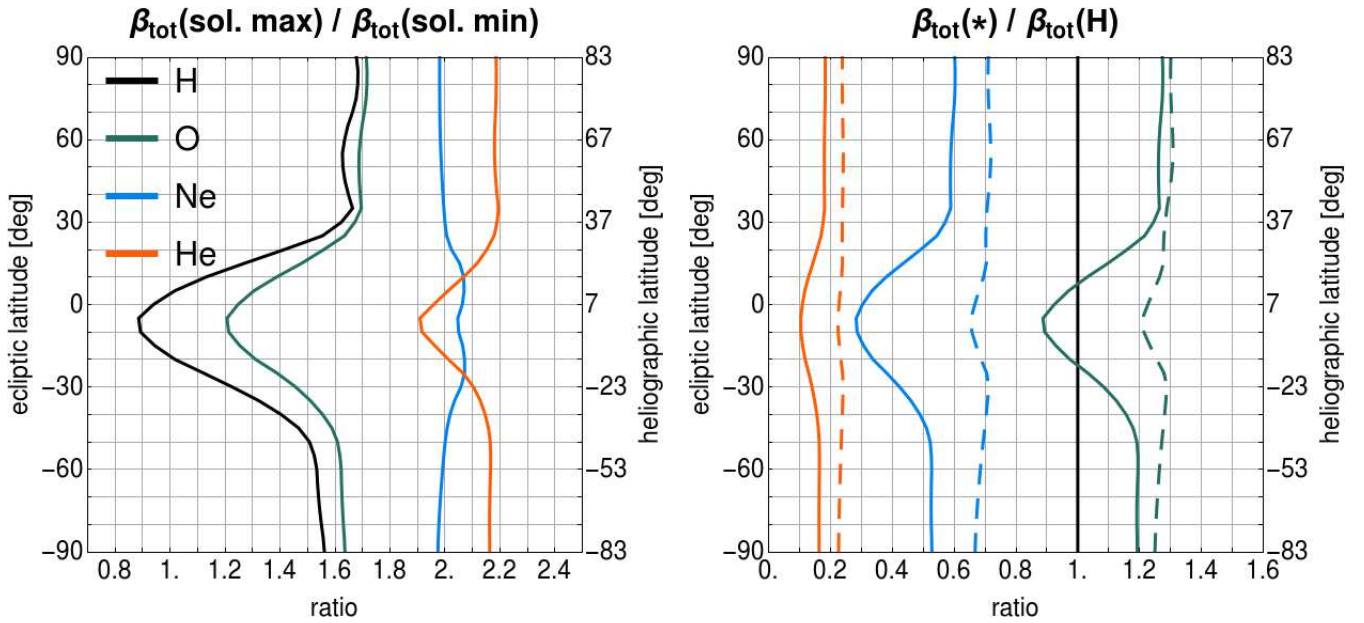


**Figure 7.** Left: ratio of the latitudinal profiles of the total ionization rates during solar maximum ( $\sim 2001$ ) to solar minimum ( $\sim 1996$ ) for H, O, Ne, and He. Right: ratio of the total ionization rates for O, Ne, and He to the total ionization rates for H as a function of latitude during solar minimum (solid line) and solar maximum (dashed line); color scheme as in the left panel.

sented in Figures 5, 6, 7, and 8. The total ionization rates for H and O are almost uniform in latitude during the solar maximum, and bi-modal for other phases of solar activity, with higher ionization rates for the inecliptic band, and lower ionization rates at higher latitudes.

For neon, the total ionization rates show an almost uniform latitudinal structure regardless of the phase of the solar activity (Figure 6). This is because for neon the dominant ionization reaction is photoionization (Table 1), for which the latitudinal variations are poorly investigated (see Section 2.2, Equation 4, and discussion in Bzowski et al. (2013b)).

For helium, photoionization is the most significant ionization reaction, but as shown in Figure 3 and Table 1, electron impact ionization may contribute significantly and thus add latitudinal variations in time to the total ionization rates (Figure 6 and 7). Since, as pointed out in Section 2.3, the significance of the electron impact ionization rate strongly increases with the decrease of the solar distance (Figure 1 and 4; Bzowski et al. (2013b,a); McMullin et al. (2004)), therefore, the latitudinal anisotropy of electron impact ionization for all species also increases with the decrease of solar distance during low and moderate solar activity.

Consequently, the total ionization rates vary significantly both in time and in latitude. The variations in

time of the latitudinal profiles of total ionization rates are presented in Figures 6 and 7 for selected epochs, and in Figure 5 for H and O the full period 1985-2018 is presented. The total ionization rates are approximately 2 times higher during solar maximum than during solar minimum for He and Ne almost regardless the latitude (Figure 7). In the case of H and O, the total ionization rates at mid and high latitudes are about 1.5 higher during solar maximum than during solar minimum (Figure 7). The in-ecliptic total ionization rates for O vary about 20% during the solar cycle with higher rates during solar maximum, and for H the variations are about 10% with higher rates during solar minimum as presented in Figure 6 and left panel in Figure 7. Interestingly, during solar minimum the ionization rates for H close to the solar equator can be greater than during solar maximum. This is a result of the long-term changes in the solar wind flux at time scales longer than the solar cycle period (see discussion in, e.g., McComas et al. (2008b) and Sokół et al. (2013)).

The amplitude of pole-to-ecliptic variations with the solar cycle is the greatest for hydrogen, and the smallest for neon as illustrated in left panel in Figure 7. During solar maximum the total ionization rates are higher at all latitudes for oxygen, neon, and helium as illustrated in Figure 6. An exception is hydrogen, for which the total ionization rate increases during solar maximum for all latitudes except a few degrees around the solar equator. As already mentioned, such variations are result of joint variations of the solar wind latitudinal structure with solar activity and long-term changes of the in-ecliptic solar wind unrelated with the solar cycle.

Table 2 compares the total ionization rates for various species with respect to total ionization rates for hydrogen both in the ecliptic plane and in the polar region. For polar regions the total ionization rates are the greatest for oxygen and are almost 30% greater than for hydrogen. Similarly, in the case of helium and neon, the polar total ionization rates are higher for polar regions than for the ecliptic rates when compared to hydrogen. The relation of the total ionization rates as a function of latitude between O, Ne, and He compared to H is illustrated for two moments in time in the right panel of Figure 7 and for the last three solar cycles in the right panel of Figure 8. The total ionization rates for oxygen are the strongest at the mid and high latitudes among all the species discussed, regardless of the phase of the solar activity.

#### 4. SUMMARY AND CONCLUSIONS

We discussed the ionization processes relevant for the ISN hydrogen, oxygen, neon, and helium inside the heliosphere. We focused on modulations in time, with solar distance, and with latitude. We discussed similarities and differences in ionization processes for the given species. We studied the relations between the total ionization rates both in the ecliptic plane and in the polar regions. Figure 8 summarizes the total ionization rates for the species discussed at 1 au in the ecliptic plane (left panel) and for the solar poles (right panel) in the period from 1985 to 2018.

The study shows that for hydrogen and oxygen the solar ionization is the strongest, and thus the resulting modulation of the H and O fluxes of heliospheric particles is expected to be the highest. The lowest modulation by solar ionizing factors is for helium, it is almost an order of magnitude smaller than for hydrogen and oxygen at 1 au and in the ecliptic plane. For He and Ne, the main source of ionization losses is photoionization, and thus ionization modulation for these species is correlated with the solar cycle variations. Hydrogen atoms are prone to the solar wind variations both in time and in latitude because charge exchange is the dominant ionization reaction for it. Oxygen is a species for which both charge exchange and photoionization losses can be dominant ionization source depending of the phase of solar activity and long-term changes in the solar wind. The total ionization rates are the highest out of the ecliptic plane for oxygen. Relative contributions of individual reactions to the total rates for the four species discussed significantly vary with latitude as a function of the phase of solar cycle, and also aperiodically due to long-term variations in the solar wind density.

The solar ionizing factors act differently on different heliospheric particles, which results in different modulation of these particles throughout the heliosphere. This brings important consequences for the study of heliospheric particles, like the ISN gas, PUIs and ENAs, as well as physical processes in the inner and outer heliosphere, as discussed by Sokół et al. (0000b,c) for the ISN gas density distribution and PUI production rate inside the heliosphere.

The presented study is supported by the Polish National Science Center grant No. 2015/19/B/ST9/01328. The IPS observations were made under the solar wind program of the ISEE.

#### REFERENCES

- |   |   |
|---|---|
| <p>Barnett, C. F., Hunter, H. T., Kirkpatrick, M. I., et al. 1990, Atomic data for fusion. Collisions of H, H<sub>2</sub>, He and Li atoms and ions with atoms and molecules, Vol. ORNL-6086/V1 (Oak Ridge, Tenn.: Oak Ridge National Laboratories)</p> | <p>Bochsler, P., Kucharek, H., Möbius, E., et al. 2014, ApJS, 210, 12</p> |
|---|---|

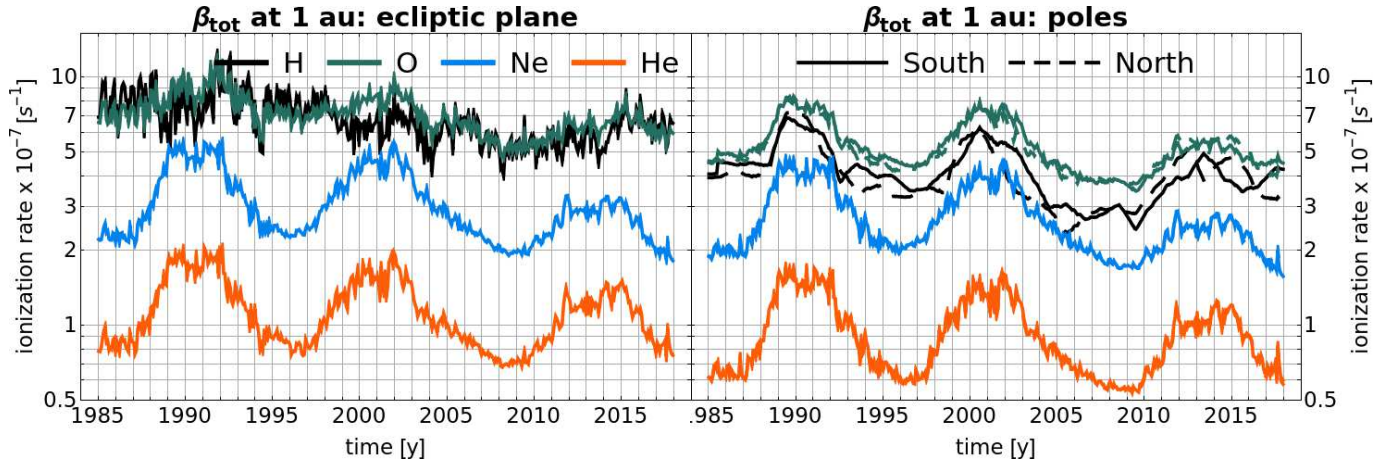


**Figure 8.** Left: times series of the total ionization rates for the four species discussed in the ecliptic plane at 1 au (see the red line in Figure 3). Right: total ionization rates at 1 au at ecliptic poles (solid line - South pole, dashed line - North pole, note: the dashed lines are indistinguishable for O, Ne, and He).

Bzowski, M. 2008, *A&A*, 488, 1057  
 Bzowski, M., Kubiak, M. A., Hlond, M., et al. 2014, *A&A*, 569, A8  
 Bzowski, M., Sokół, J. M., Kubiak, M. A., & Kucharek, H. 2013a, *A&A*, 557, A50  
 Bzowski, M., Sokół, J. M., Tokumaru, M., et al. 2013b, in *Cross-Calibration of Far UV Spectra of Solar Objects and the Heliosphere*, ed. E. Quémerais, M. Snow, & R. Bonnet, ISSI Scientific Report No. 13 (Springer Science+Business Media), 67–138  
 Bzowski, M., Swaczyna, P., Kubiak, M., et al. 2015, *ApJS*, 220, 28  
 Fahr, H., Fichtner, H., & Scherer, K. 2007, *Rev. Geophys.*, 45, RG4003  
 Fox, N. J., Velli, M. C., Bale, S. D., et al. 2016, *SSRv*, 204, 7  
 Judge, D. L., McMullin, D. R., Ogawa, H. S., et al. 1998, *SoPh*, 177, 161  
 King, J. H., & Papitashvili, N. E. 2005, *J. Geophys. Res.*, 110, 2104  
 Kowalska-Leszczynska, I., Bzowski, M., Sokół, J. M., & Kubiak, M. A. 2018a, *ApJ*, 852, 15  
 —. 2018b, *ApJ*, 0000, 00  
 Le Chat, G., Issautier, K., & Meyer-Vernet, N. 2012, *SoPh*, 279, 197  
 Lindsay, B. G., & Stebbings, R. F. 2005, *J. Geophys. Res.*, 110, A12213  
 Lotz, W. 1967, *Z. Phys.*, 206, 205  
 McComas, D., Allegrini, F., Bagenal, F., et al. 2008a, *SSRv*, 140, 261  
 McComas, D., Bzowski, M., Frisch, P., et al. 2015, *ApJ*, 801, 28

McComas, D. J., Christian, E. R., Schwadron, N. A., Fox, N., et al. 2018a, *SSRv*, 000, 000  
 McComas, D. J., Ebert, R. W., Elliot, H. A., et al. 2008b, *Geophys. Res. Lett.*, 35, L18103  
 McComas, D. J., Allegrini, F., Bochslers, P., et al. 2009, *SSRv*, 146, 11  
 McComas, D. J., Dayeh, M. A., Allegrini, F., et al. 2012, *ApJS*, 203, 1  
 McComas, D. J., Allegrini, F., Bzowski, M., et al. 2014, *ApJS*, 213, 20  
 McComas, D. J., Dayeh, M. A., Funsten, H. O., et al. 2018b, *ApJL*, 856, L10  
 McMullin, D. R., Bzowski, M., Möbius, E., et al. 2004, *A&A*, 426, 885  
 Möbius, E., Lee, M. A., & Drews, C. 2015, *ApJ*, 815, 20  
 Nakai, Y., Shirai, T., Tabata, T., & Ito, R. 1987, *Atomic Data and Nuclear Tables*, 37, 69  
 Park, J., Kucharek, H., Möbius, E., et al. 2014, *ApJ*, 795, 97  
 Ruciński, D. 1985, PhD thesis, Centrum Badań Kosmicznych PAN  
 Ruciński, D., Bzowski, M., & Fahr, H. J. 1998, *A&A*, 334, 337  
 Ruciński, D., Cummings, A. C., Gloeckler, G., et al. 1996, *SSRv*, 78, 73  
 Ruciński, D., & Fahr, H. J. 1989, *A&A*, 224, 290  
 —. 1991, *Ann. Geophys.*, 9, 102  
 Scherer, K., Fichtner, H., Fahr, H.-J., Bzowski, M., & Ferreira, S. E. S. 2014, *A&A*, 563, A69  
 Snow, M., Weber, M., Machol, J., Viereck, R., & Richard, E. 2014, *Journal of Space Weather and Space Climate*, 4, A04  
 Sokół, J. M., & Bzowski, M. 2014, *ArXiv e-prints*, arXiv:1411.4826



- Sokół, J. M., Bzowski, M., Kubiak, M., & McComas, D. J. 0000a, ApJ, in preparation
- Sokół, J. M., Bzowski, M., Kubiak, M., & Möbius, E. 2016, MNRAS, 458, 3691
- Sokół, J. M., Bzowski, M., Tokumaru, M., Fujiki, K., & McComas, D. J. 2013, SoPh, 285, 167
- Sokół, J. M., Kubiak, M., Bzowski, M., & Kowalska-Leszczynska, I. 0000b, ApJ, in preparation
- Sokół, J. M., Swaczyna, P., Bzowski, M., & Tokumaru, M. 2015, SoPh, 290, 2589
- Sokół, J. M., Bzowski, M., Grygorczuk, J., et al. 0000c, ApJ, in preparation
- Tapping, K. F. 1987, J. Geophys. Res., 92, 829
- . 2013, Space Weather, 11, 1
- Tarnopolski, S., & Bzowski, M. 2009, A&A, 493, 207
- Tokumaru, M., Fujiki, K., & Iju, T. 2015, J. Geophys. Res., 120, 3283
- Tokumaru, M., Kojima, M., & Fujiki, K. 2010, J. Geophys. Res., 115, A04102
- . 2012, Journal of Geophysical Research (Space Physics), 117, 6108
- Tokumaru, M., Shimoyama, T., Fujiki, K., & Hakamada, K. 2018, J. Geophys. Res., 123, 2520
- Verner, D. A., Ferland, G. J., Korista, T. K., & Yakovlev, D. G. 1996, ApJ, 465, 487
- Wenzel, K.-P., Marsden, R. G., Page, D. E., & Smith, E. J. 1989, Adv. Space Res., 9, 25
- Wieman, S. R., Didkovsky, L. V., & Judge, D. L. 2014, SoPh, 289, 2907
- Witte, M., Rosenbauer, H., Keppler, E., et al. 1992, A&AS, 92, 333
- Woods, T. N., Rottman, G. J., White, O. R., Fontenla, J., & Avrett, E. H. 1995, ApJ, 442, 898
- Woods, T. N., Eparvier, F. G., Bailey, S. M., et al. 2005, J. Geophys. Res., 110, A01312
- Young, D. T., Berthelier, J. J., Blanc, M., et al. 2004, SSRv, 114, 1
- Zank, G. P. 2015, ARA&A, 53, 449